The Development and Application of an Arctic Sea Ice Emulator v.1

Sian Megan Chilcott [1,2] and Malte Meinshausen [1]

[1]School of Earth and Atmospheric Science, The University of Melbourne, Parkville 3010, Victoria, Australia
[2]Max-Planck-Institute for Meteorology, Universität Hamburg, Hamburg, 20146, Germany

Correspondence: Sian Megan Chilcott (smchilcott@student.unimelb.edu.au)

Abstract. The high computational expense of complex climate models and their tendency to underestimate observational records of Arctic sea ice sensitivity to anthropogenic forcers, challenge our ability to assess the magnitude of forcing that will cause Arctic sea ice loss to cross critical thresholds. To address these limitations, we development an Arctic sea ice emulator, that is calibrated to the response of sea ice area to global warming in physically-based CMIP6 models and constrained to

5   observations. Our constrained emulator reduces the remaining budget of CO_2 that can be emitted to prevent seasonally ice-free conditions from $821GtCO_2$ by CMIP6 multi-model ensemble estimates to $380GtCO_2$. This suggests that limiting global warming to $1.5°C$ is sufficient to prevent a seasonally ice-free Arctic Ocean, whereas $2°C$ proves insufficient. Our results also provide insight into the future of winter sea ice over a greater ensemble range than previously possible, pinpointing the emission threshold at which the ice pack detaches from land, after which the ice pack rapidly disappears to year-round ice free

10   conditions.

1 Introduction

Arctic sea ice forms a complex yet fundamental component of the Earth system and is a sensitive indicator of global climatic changes. Since the satellite record began in 1979, the September ice pack has declined by more than 13% per decade in response to anthropogenic greenhouse gas emissions (Serreze and Stroeve, 2015).

15 Global climate models (GCMs) used in the most recent (sixth) phase of the Coupled Model Intercomparison Project (CMIP), are the most comprehensive tools we have for predicting how Arctic sea ice will change in the future. Their projections unanimously show continued year-round reductions in Arctic sea ice throughout the 21st century, with the majority of models projecting a seasonally ice-free Arctic Ocean within the next 15 to 50 years, commonly defined as the first time SIA falls below 1 million km^2 in a given month (SIMIP Community, 2020). Though models agree ice loss will persist into the future, there are
20 large uncertainties surrounding their projections (SIMIP Community, 2020). One conceptually convenient metric to measure changes in sea ice is the 'sea ice sensitivity', which is generally defined as the amount of sea ice area lost per degree of global warming. However, GCMs tend to simulate a lower sensitivity of Arctic summer sea ice loss than has been observed (Mahlstein and Knutti, 2012; Rosenblum and Eisenman, 2017; Niederdrenk and Notz, 2018; SIMIP Community, 2020). Models that do simulate present day rates of sea ice loss also simulate considerably higher global warming than observations suggest
25 (Rosenblum and Eisenman, 2017). This is known as the 'hot model' problem and is used to describe models that project climate warming in response to CO_2 emissions that is much larger than other lines of evidence suggest (Hausfather et al., 2022). Recent observations report the Arctic Amplification, defined as the warming ratio between the Arctic and global temperature, over the satellite period has warmed much faster than in CMIP6 models which tend to simulate a relatively constant Arctic Amplification over the 21st century (Chylek et al., 2022; Rantanen et al., 2022; Douville, 2023; Chylek et al., 2023; Hay et al.,
30 2024).

The majority of CMIP6 models limit runs to 2100 as they are too computationally expensive to analyse large numbers of scenarios over multi-centennial timescales (Balaji et al., 2017). A few studies have utilised the limited number of extended simulations, to analyse the winter sea ice response to warming, using the limited subset of available models with extended simulations to 2300, with particular interest in the possibility of a rapid disappearance of winter sea ice (Armour et al., 2011;
35 Hezel et al., 2014; Bathiany et al., 2016; DeRepentigny et al., 2020; Hankel and Tziperman, 2021, 2023). These studies found that the linear decline of Arctic sea ice with cumulative CO_2 emissions to ice-free conditions exhibited through the summer months breaks down in winter. Arctic sea ice declines at a much slower rate in winter before reaching a threshold at which the amount of sea ice loss per emitted ton of CO_2 rapidly increases. A recent study from Ritschel (2024) attributes the rapid loss of Arctic winter sea ice to the detachment of the ice pack from land. They ascertain that the detachment of the ice pack
40 from land is linked to the timing of geographic muting, a term introduced by Eisenman (2010) to describe the blocking of the ice pack's expansion through the growth season, due to the presence of land masses surrounding the Arctic Ocean. This mechanism explains the slow decline of winter sea ice initially, as the theoretical retreat of winter sea ice is masked by the coastline. This causes the area of the coast bound ice to change minimally. Once the temperature becomes sufficiently high

to prevent the ice pack expanding to the coastline, the ice pack has 'detached' from land and exhibits a higher sensitivity to
warming (Ritschel, 2024). As the timing of rapid winter ice loss tends to occur after the end of the 21st century, the lack of
extended projections in CMIP6 models prevents a thorough analysis of winter ice loss.

This study therefore aims to address three key gaps in the literature. The first fundamentally seeks to build on and extend the
insights we gain from comprehensive, higher complexity model runs to emulate the CMIP6 response of Arctic sea ice area to
global warming in all months at a much smaller computational expense. In a second step we aim assess whether the calibration
of our parameterisations to CMIP6 models between 1850 and 2100, capture the non-linearity of winter sea ice when extended
to 2300. Finally, this study aims to assess whether the sensitivity of sea ice loss to global warming can be constrained to match
the observed, through bias corrections to the global warming and Arctic Amplification trends. This approach aims to integrate
various lines of evidence to efficiently emulate plausible, long-term projections of SIA under a range of SSP scenarios.

2 Arctic Sea Ice Emulator Setup

2.1 Model Description Overview

Our emulator setup is separated into two stages which are each comprised of three steps (fig. 1). Stage one involves param-
eterisation development and calibration to CMIP6 data, while stage 2 constrains our CMIP6 informed parameterisations to
observations. Within each stage, step i emulates the Arctic Amplification, converting the global annual mean temperature to
the Arctic annual mean temperature. Step ii emulates the Arctic seasonal temperature cycle which converts our emulated Arc-
tic mean temperature to the Arctic seasonal temperature and is then input into the sea ice parameterisation in step iii. In the
first stage, parameterisations have been calibrated over the period 1850-2100 against the corresponding first ensemble member
of 12 selected CMIP6 models for the scenarios SSP5-8.5, SSP 2-4.5 and SSP1-2.6 and their historical runs. We chose these
scenarios and calibration period based on the availability of both CMIP6 temperature and SIA projections. In the second stage
we force our emulator with the MAGICC 600-member ensemble that has been constrained to represent the IPCC AR6 WG1
global warming projections and their uncertainty (Cross-Chapter Box 7.1, IPCC (2021) AR6 WG1; Nicholls et al. (2021)).
We combine the MAGICC ensemble with our probabilistic constraint on Arctic Amplification in step ii, which we then pass
through remaining steps to produce constrained, probabilistic projections of SIA to 2300. Given that we emulate the sea ice
response with parameterisations that smooth out year to year variability, we prioritise the development of our emulator's capa-
bility to represent structural variability. Our emulation approach therefore does not attempt to capture the year to year natural
variability of Arctic sea ice, rather the long-term median Arctic sea ice response. This is because the contribution from internal
processes to the overall variability reduces in long-term sea ice projections, while the contribution from structural and scenario
variability contribute greater significance to the long-term sea ice projections (Bonan et al., 2021).
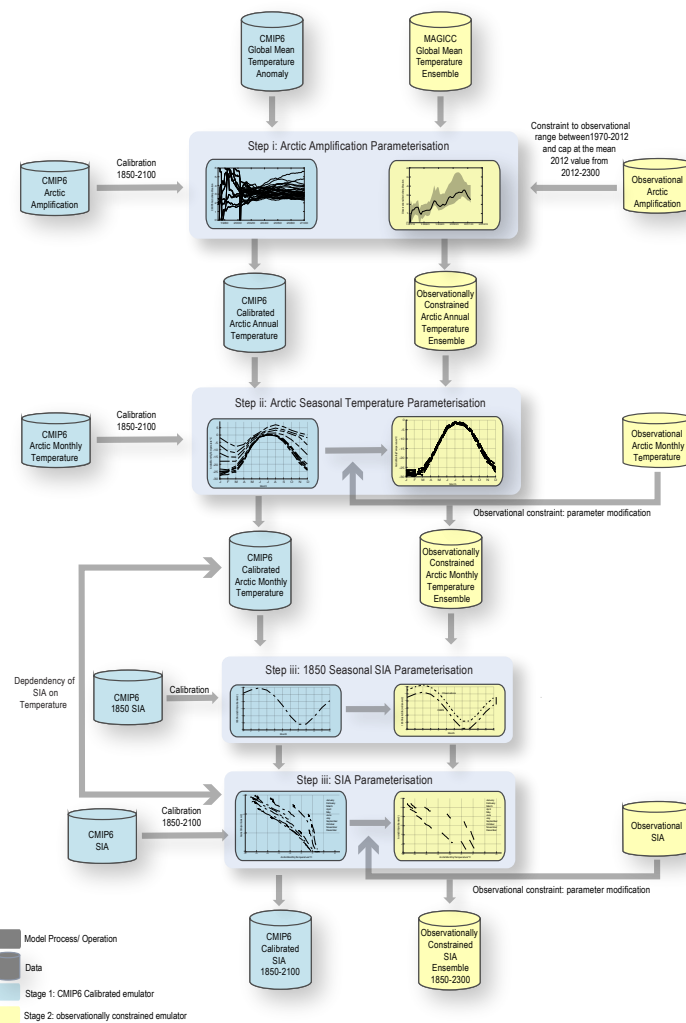
Figure 1. Conceptual model of emulator development.

2.2 Model Calibration

The calibration routine utilises the Nelder and Mead simplex optimisation method (Nelder and Meadf, 1965; Lagarias et al.,
75 1998), with a termination tolerance of 10^{-6} and a maximum iteration of 1000. We use the residual sum of the squared dif-
ferences (RSS) for goodness-of-fit (GOF) diagnostics during the optimization process. This setup iteratively evaluates the
calibration factor values to ensure they result in an RSS global minimum between the CMIP6 data (with a running mean of 10
years applied) and the emulated data. The optimisation routine is initialised via a number of preliminary runs to generate a se-
ries of starting parameters, by randomly sampling values from a set of user-defined ranges for each parameter. Each calibrated
80 parameter in the final model-specific set is designed to control all months in each model.

2.3 Step i: The Arctic Amplification Parameterisation
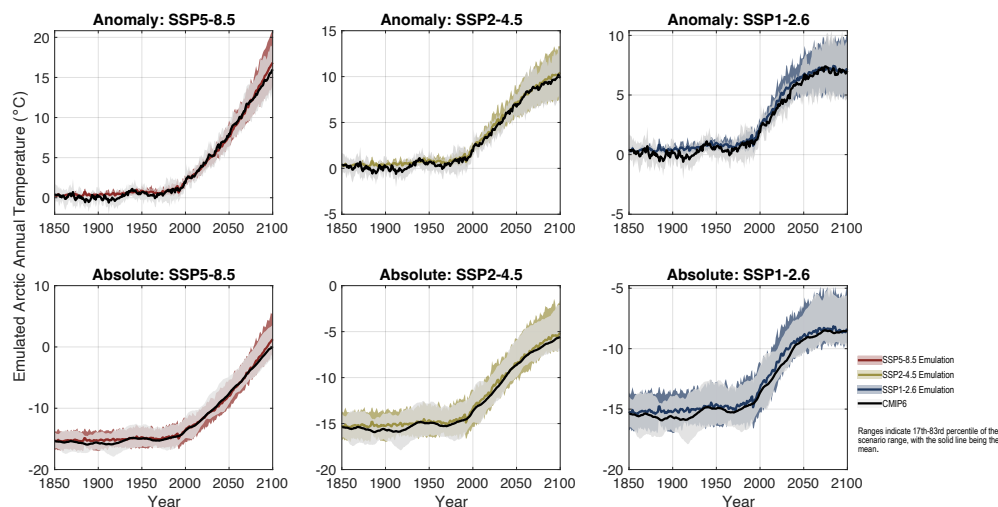
Figure 2. Emulation of CMIP6 calibrated Arctic annual mean temperatures. The top row represents the calibrated temperature anomaly,
while the bottom row represents the calibrated absolute temperature. Red, yellow and blue shading represents the SSP5-8.5, SSP2-4.5 and
SSP1-2.6 *likely* (17th-83rd percentile) calibrated range, with darker solid lines representing the mean in each scenario. Light grey shading
represents the CMIP6 *likely* range and solid black lines represent the CMIP6 multi-model median.

In stage 1, we force our emulator with the global mean temperature anomaly from each of the CMIP6 models used in this study.
We split the emulation of the Arctic temperature into two parameterisations- annual (step i) and seasonal Arctic Amplification

(step ii). Splitting these processes provides the basis for the observational constraint of annual Arctic Amplification in stage 2

85 of emulator development.

We find that a simple linear regression between the global and Arctic annual mean temperature anomaly, $tas_{(AAAB)} = \beta \cdot (tas_{(GAB)} - tas_{(GREF)}) + tas_{(AREF)}$, over the calibration period is sufficient to emulate the CMIP6 Arctic annual mean surface temperature (fig. 2). Where $tas_{(AAAB)}$ is the output Arctic annual absolute temperature, $tas_{(GAB)}$ is the global absolute temperature, $tas_{(GREF)}$ is the average 1850-1900 global absolute temperature and $tas_{(AREF)}$ is the average 1850-1900 Arctic

90 absolute temperature, $(tas_{(GAB)} - tas_{(GREF)})$ represents the global mean temperature anomaly and β is the regression coefficient representing the Arctic Amplification factor with a range between 2.5 and 4 about a median of 3, and is derived from the linear regression between the global mean and Arctic annual mean temperature anomaly. To generate the absolute temperature ($tas_{(AAAB)}$), the 1850-1900 mean Arctic absolute temperature ($tas_{(AREF)}$) for the first ensemble member of each CMIP6 model was added to the Arctic annual mean temperature anomaly ($\beta \cdot (tas_{(GAB)} - tas_{(GREF)})$), to produce CMIP6 absolute

95 temperatures.

2.3.1 Observational Constraint on Arctic Amplification
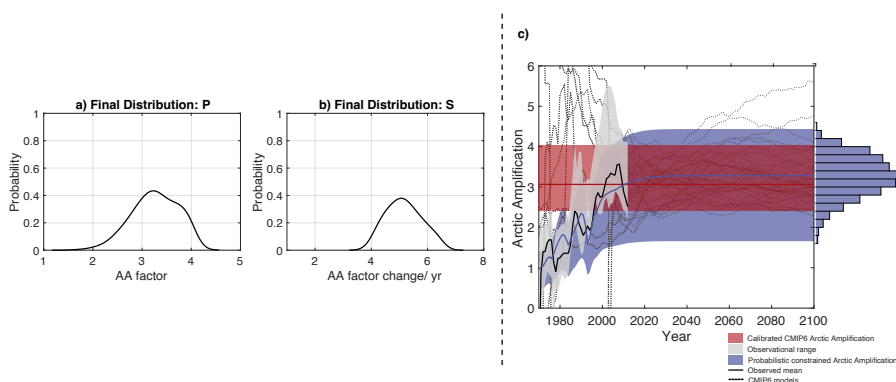
Figure 3. Our Arctic amplifications parameterisation as presented in Eq. (1). Light grey shading represents the *'very likely'* (5th-95th percentile) observational Arctic Amplification range, where the black solid line is the observational mean. Red shading represents the *'very likely'* CMIP6 calibrated Arctic Amplification range, where the red solid line is the CMIP6 calibrated multi-model mean. Blue shading represents the final Arctic Amplification uncertainty range. We take 2012 as the final year of observations, as it is the last year a central point can be taken with 10 years either side to calculate the 21-year trend without reducing the number of years in the trend, which could bias the trend of the final years.

Given the disparity between simulated and observed Arctic Amplification trends, a more complex approach is required to constrain model trends to align with observational data. We note that due to the poor signal to noise ratio, we require warming to reach 0.45°C over a 20-year period before deriving Arctic Amplification from the observational record. As such, we focus

100 our analysis on Arctic Amplification trends from 1970. The resultant parameterisation of our constraint on Arctic Amplification is as follows:

$$\text{Arctic Amplification}_{r,p,s} = \frac{p}{(1 + \exp\left(s \cdot (-r + 0.5)\right))}. \tag{1}$$

Equation (1) is a sigmoid that initially assumes a linear increase of Arctic Amplification with global mean temperature at a rate dictated by s, which progresses asymptotically towards a constant Arctic Amplification prescribed by the parameter p,

105 after which the amplification factor will remain constant as warming continues. r represents a randomly sampled MAGICC global mean temperature ensemble member, while its negative sign $(-r)$ indicates that the sigmoid should increase rather than decrease with warming. We add a fixed factor of 0.5 to the exponential term to control the temperature at which the Arctic Amplification begins to increase, as the observed Arctic Amplification rises from a mean of approximately 1 as warming grades rise above 0.45°C (fig. 3). The division of p with the non-linear exponential term on the denominator, $(1 + \exp\left(s(-r) + 0.5\right))$,

110 controls the sigmoidal increase of Arctic Amplification with global warming at a rate prescribed by observations, while remaining constant thereafter to account for the modelled CMIP6 trend (see Supplementary Sect. S1.1).

2.4 Step ii: The Arctic Seasonal Temperature Parameterisation

We develop our seasonal temperature parameterisation to reflect three 'key features' of warming on the evolution of the seasonal temperature cycle. The first is the asymmetric warming between summer and winter which gradually reduces the amplitude

115 of the seasonal temperature cycle over the calibration period (fig. 4). Secondly, the pre-industrial period (1850-1900) seasonal temperature cycle is relatively symmetrical as the rate of warming from winter to summer is similar in magnitude to the rate of cooling back to winter. However, as the Arctic warms and sea ice declines, the temperature cycle widens at its peak as the melt season lengthens and warm summer temperatures persist into the autumn months. Finally, we find the temperature amplification is not linear in all months. From the mid-21st century the temperature amplification increases during the summer

120 months (June-August), declines in autumn and early winter (September-January), and remains relatively constant through late winter and spring (February-April) (Supplementary fig. S2). The likely cause of the seasonal amplification difference is outlined by Dai et al. (2019), and is related to the seasonal exchange of fluxes between the ocean surface and atmosphere, which respond differently to variations in the rate of sea ice loss to rising CO_2 emissions. We represent these trends via a nested, exponential cosine function that emulates the shape of the seasonal temperature curve in each year, and is controlled

125 by the Arctic annual mean temperature:

$$P = f \cdot (\cos(m \cdot g - e \cdot \exp\left(\cos(m^a)\right))), \tag{2a}$$

$$tas_{(AMAB)} = P + h, \qquad\qquad (2b)$$

where $tas_{(AAAB)}$ is the Arctic annual mean temperature in degrees Celsius emulated in step i, m is an equally spaced value be-

130 tween 0 and 2π representing each month of the year (0 and 2π represent January of year t and January of year $t+1$ respectively) and f, g, and a are model-specific calibration parameters dependent on the Arctic annual mean temperature. f represents the amplitude, g controls the wavelength, while a (Eq. 2c) is a simple cosine function that controls the change from a basic cosine curve to a shallow, linear temperature decline, as warmer summer temperatures gradually pervade into September, October, November and December (Supplementary fig. S3). e is a non-temperature dependent and non-model specific parameter with

135 a value of 0.3, that fixes the phase shift of the curve and therefore controls the rate of change from summer to winter temperatures. Finally, h (Eq. 2d) is a non-optimised parameter that moves the temperature curve vertically to ensure the emulated Arctic annual mean temperature input at time t is equal to the mean of the parameterised monthly temperature curve and is calculated at every time step. f and g are calculated from the calibration coefficients f_1, f_2, g_1 and g_2 that are optimised through a series of simple linear regression dependent on the Arctic annual mean temperature; ($f = (f_1 \cdot tas_{(AAAB)}) + f_2$) and g

140 $= (g_1 \cdot tas_{(AAAB)}) + g_2$, Supplementary table. S1) We acknowledge that while f and g are related, the complexity of the system did not allow us to find a functional form to capture their relationship. As such, we handle these two parameters separately.

$$a = \cos((tas_{(AAAB)} \cdot -a_1) - a_2) + a_3, \qquad\qquad (2c)$$

$$h = \frac{tas_{(AAAB)} - \overline{P}}{f}. \qquad\qquad (2d)$$

The first key feature (see above) is encapsulated by parameter f, which reduces the amplitude of the curve with warming.

145 The second is satisfied by the exponent of the cosine $\exp(\cos(m^a))$. This feature lengthens the summer season as the Arctic annual mean temperature increases. Although our function initially assumes a basic cosine curve at lower values of $tas_{(AAAB)}$, this feature creates the increasingly asymmetric and broad peaked curve as $tas_{(AAAB)}$ rises, generating a left skewed curve at higher Arctic annual mean temperatures. Finally, adding the exponent into the nested cosine $(\cos(m(\cos(m^a))))$ prevents the temperature in the autumn months rising as fast as the winter months, reducing the amplification from the mid-21st century

150 while simultaneously increasing the amplification during summer. The combined decline in amplitude (f) and increase in wavelength (g) prevents the increase in summer amplification initially, however as the wavelength increases the curve becomes
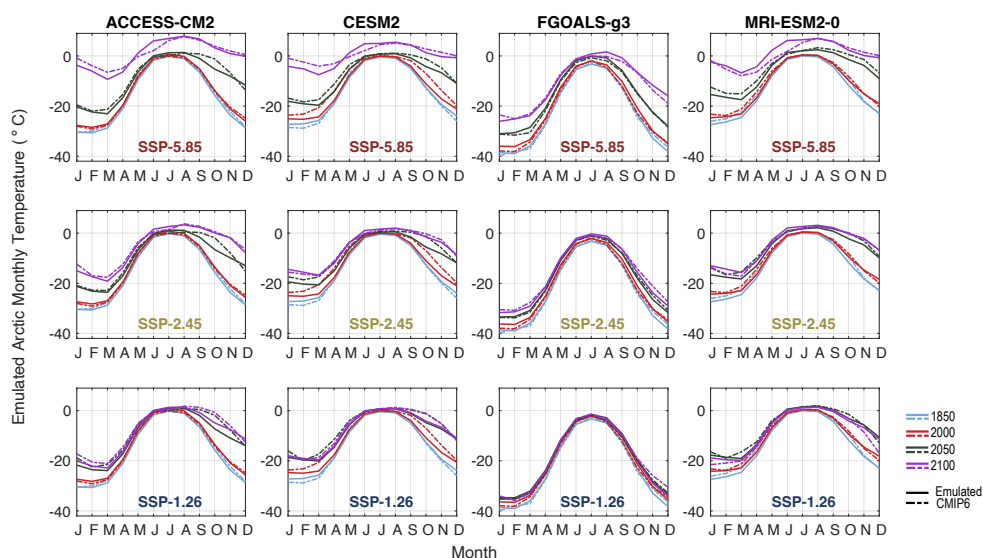
Figure 4. Emulation of the CMIP6 Arctic seasonal temperature cycle in 4 selected years and models. Each column represents our emulation of one model, where the top, middle and bottom rows represent SSP5-8.5, SSP2-4.5 and SSP1-2.6 respectively. Solid lines represent our emulation of a selected CMIP6 model and dashed lines of the same colour represent the CMIP6 data. Only emulation of the years 1850, 2000, 2050 and 2100 are are displayed for visualisation purposes, however calibration was conducted over each year between 1850 and 2100, were one year represents one curve.

more left skewed causing the rate of July and August warming to increase. This satisfies the third key feature of the seasonal temperature evolution we identify in CMIP6 models.

Analysis of the few models with runs to 2300 (CanESM5), show the shape of the temperature curve doesn't evolve significantly

155 past 2100. As such, we cap the evolution of our calibration parameters to ensure they remain constant past an Arctic annual mean temperature of 6°C (Supplementary fig. S4). Past this temperature, h (Eq. 2d) is the only parameter that continues to change. We find the temperature parameterisation produces a plausible timeseries to 2300 using this method (Supplementary fig. S5).

2.4.1 Bias Corrections to Arctic Monthly Temperature Parameterisation

160 CMIP6 projections of the mean 1979-2020 Arctic summer (April-July) temperatures are on average warmer 2°C than observed (Supplementary fig. S6). To overcome this, we apply a constant offset to our CMIP6 calibrated temperature in each month, which is we define as the difference between the 1979-2020 mean from observations and that of our emulation. We acknowledge the 1979-2020 period is a short time frame and internal variability could be a large factor causing this difference. However, as future observations become available and the impact of internal variability is better understood, this bias correction can be

165 updated in future versions of our emulator.

CMIP6 models also project a weaker summer (July and August) warming trend than is observed (Supplementary fig. S6). Simulated July and August temperatures increase slowly from 1980 to 2050 before rising significantly thereafter, whereas observed temperatures rise rapidly from ~1980. We address this by forcing the calibration parameter 'f', which represents the amplitude of the temperature curve in each year in Eq. (2b), to remain constant until the annual mean Arctic temperature

170 reaches an absolute level of -8°C. Our bias correction ensures the summer temperatures increase at the observed rate, while protecting our emulation of the lengthening melt season (Serreze and Barry, 2011).

2.5 Step iii: The SIA Parameterisation

We parameterise the response of Arctic sea ice area to the seasonal Arctic warming trend, as this is ultimately the temperature sea ice responds to (as opposed to global-average warming itself). As CMIP6 models reproduce the observed Arctic warming

175 trend well, this method also ensures our SIA projections respond to Arctic warming trends that match the observed, reducing the number of bias corrections in stage 2.

2.5.1 The Seasonal Melt and Growth Weighting Scheme

The response of Arctic sea ice to temperature is impacted by many different physical processes such as snow cover and ocean heat content changes. Variations in sea ice thickness in particular offers insight into how the different rate of ice area growth

180 and melt can be incorporated into our emulator. During autumn freeze-up, a thin layer of sea ice will rapidly form over the Arctic Ocean. However, during the melt season, a greater thickness of ice needs to melt before the SIA is greatly affected. This produces a differing inertia to temperature changes between the growth and melt of SIA, where for a given temperature change the loss or gain of SIA will be greater in autumn compared to that of spring. We therefore apply a weighting scheme to the emulated temperature that forces our SIA parameterisation, to account for the inertia in the sea ice system (Supplementary fig.

185 S7). The updated temperature ('tas') therefore becomes a product of the current month, $tas_{(m)}$ and the previous month, and is computed via the following weighting scheme:

$$tas_{(new)} = \frac{(tas_{(m)} \cdot w_1) + (tas_{(m-1)} \cdot w_2)}{w_1 + w_2}, \tag{3a}$$

where $tas_{(m)}$ is the Arctic temperature at the monthly timestep m, $tas_{(m-1)}$ is the temperature from the previous month and w and $1-w$ are the weightings applied to the current and previous month respectively.

190 When applying a greater weight to the previous month's temperature in spring, the updated temperature is colder as a greater weight is placed on the colder winter temperatures (Supplementary fig. S7b). Spring SIA is therefore forced with a colder temperature to express the slower decline of SIA for a given temperature change through the melt season. Whereas, the updated temperature is higher in autumn as it becomes a function of the the previous warm summer month, to capture the faster growth of sea ice for an equivalent temperature change through the growth season.

195 Due to the effect of 'geographic muting' described in Sect. 1, Arctic summer sea ice declines linearly with Arctic warming while the loss of winter sea ice accelerates with warming as the ice pack detaches from land (Ritschel, 2024). Given these characteristics, we develop the following parameterisation to reflect the sigmoidal decline of SIA with Arctic warming:

$$SIA = \frac{(SIA_{max} + d) \cdot (1 + \exp(tas_{(t=0)} - b)) - a(tas - tas_{(t=0)})}{(1 + \exp(tas - b))}, \tag{3b}$$

where SIA_{max} (Eq. 3c) is the seasonal SIA in 1850 and is optimised for each model, a, b and d are model dependent calibration
200 factors and 'tas' is the weighted Arctic seasonal temperature emulated in step ii.

The resultant functional form initially assumes a slow linear decline of SIA with temperature, which progresses asymptotically towards a constant SIA of 0 million km^2 at higher temperatures (fig. 5). Our SIA parameterisation is therefore derived from the division of a linear and non-linear ('tas') term. The linear response term on the numerator $a(tas - tas_{t=0})$ controls the initial linear decline of SIA with temperature and is scaled via the subtraction of the 'tas' in 1850 from subsequent 'tas' in each year;
205 while the exponential 'tas' term $(1 + \exp(tas - b))$ on the denominator, controls the sigmoidal decline of SIA and therefore the increase in the sensitivity of sea ice loss to warming in the colder months. The starting term $(SIA_{max} + d) \cdot (1 + \exp(tas_{(t=0)} - b))$ fixes the initial SIA in each month, and is the maximum SIA susceptible to melting. SIA_{max} is vertically shifted via d to account for the chaotic nature of pre-industrial sea ice fluctuations for small warming grades, and the imperfect nature of emulations. An exponential 'tas' term is added for the timestep 0 to account for the increase in the exponent of 'tas' as the initial temperature
210 nears 0°C in the summer months, ensuring that the maximum SIA is equal to $SIA_{max} + d$ in the summer months. The CMIP6
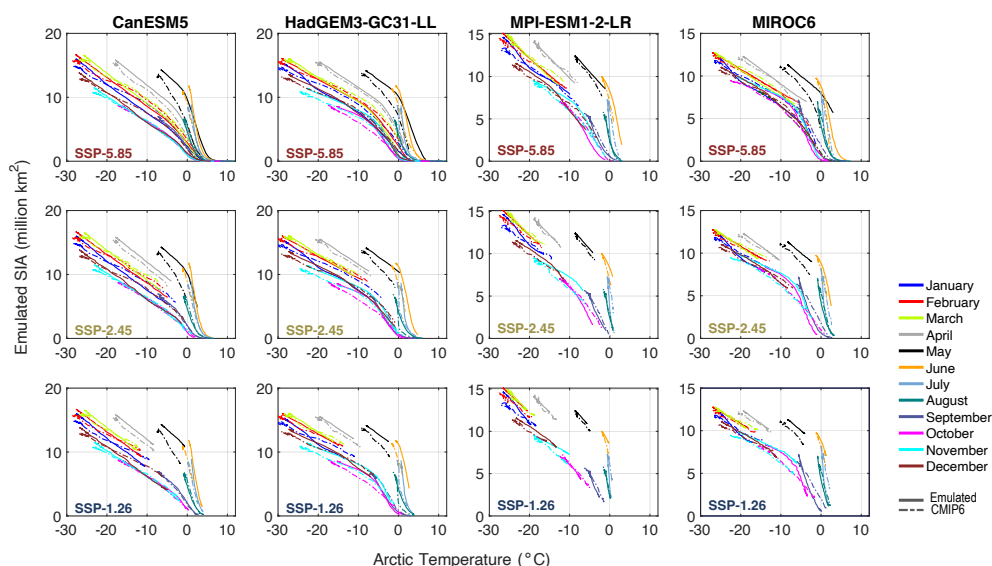
Figure 5. Emulation of the CMIP6 Arctic seasonal Sea Ice Area cycle in 4 selected models. Each column represents our emulation of the SIA under three scenarios from one CMIP6 model, where the top, middle and bottom rows represent SSP5-8.5, SSP2-4.5 and SSP1-2.6 respectively. Solid lines represent our emulation of the CMIP6 SIA in each month, and dashed lines of the same colour represent the CMIP6 data.

seasonal cycle of SIA in 1850 contains a few key features that justify the more complex adapted sine function in Eq. (3c) (Supplementary fig. S8) below:

$$\mathrm{SIA_{max}} = f \cdot (-\exp(\sin(m^g \cdot a - e))) + d, \tag{3c}$$

$$215 \quad e = (a \cdot 0.8003) + 1.5016, \tag{3d}$$

where m is again an equally spaced value between 0 and 2π representing each month of the year (0 and 2π represent January of year t and January of year t+1 respectively). Calibration factors a, f and d control the wavelength, amplitude and vertical

shift respectively. The parameter e controls the phase shift and is a constant derived from a linear regression of a. The exponent of the sine $-\exp(\sin(m^g))$ is added to flatten the trough of the curve, as August and September have similar pre-industrial values. Whereas the m^g term modulates the roundness of the peaks, to ensure the SIA increases sharply from January to its peak in March. This term allows the wavelength to capture the slow transition from winter SIA to summer SIA, while capturing the faster transition from summer SIA to winter SIA in 1850. Finally, we use a negative exponent to represent the decline in SIA through the summer months. The parameter e then adds a small phase shift to adjust the phase to each specific model. The SIA_{max} factor is first optimised and then input into the SIA calibration.

2.5.2 Bias Corrections to the Sea Ice Area Parameterisation

Similarly to the Arctic seasonal temperature bias correction, we find the modelled 1979-2014 mean SIA between June and September is on average 1.14 million km^2 smaller than observations suggest (fig. S6). To address this, we adjust SIA_{max} in each month by subtracting the difference between the 1979-2020 mean observed SIA and our emulated mean.

We also find that applying the bias-corrected temperature from Sect. 2.4.1 to our SIA parameterisation generates a much larger sea ice loss per degree of warming than is indicated by both CMIP6 models and observations (Supplementary fig. S9). This is to be expected as our corrected temperatures rise at a faster rate between 1979 and 2050 than in CMIP6 projections, while our calibrations representing the response of SIA to Arctic warming remain unchanged. This causes the sensitivity of SIA loss to increase at a cooler temperature, as the sensitivity parameter 'b' (Eq. 3b), is reached much earlier than in our calibration. To overcome this, we adjust 'b' by subtracting the difference in the mean 1979-2050 Arctic temperature produced from bias correcting the calibration parameter 'f', and the CMIP6 calibrated temperature where the calibration parameter 'f' has not been bias corrected. This approach forces the sensitivity to increase at the calibrated temperature and year that CMIP6 models suggest, while also allowing the temperatures to rise at the same rate as observations. The impact of this difference is minimal in the colder months but more pronounced in the summer, as 'b' tends to be reached before 2050 through the summer months while it is reach much later in winter.

3 Results

3.1 Assessing the Performance of our Emulator to 2300

Through this section, we evaluate the ability of our CMIP6 emulator to reproduce the CMIP6 response of SIA to warming in each month when extended to 2300, with particular focus on its ability to project the rapid disappearance of March sea ice. We note that when referring to our '2100 calibration' we refer to our calibration between 1850 and 2100, while our 'out of sample' test refers to emulator output when we force our 2100 calibrations with extended global warming projections to 2300.

We find our 2100 calibrations hold 'out of sample', projecting an ice-loss between 1850 and 2300 that aligns with the CMIP6 trend for each month and model, successfully capturing the rapid loss of March sea ice to both global and Arctic warming (fig. 6 and Supplementary fig. S11). We evaluate the goodness of fit (GOF) between our emulation of SIA to 2300 with the corresponding CMIP6 model using a weighted residual sum of squares (RMSE), divided by the number of calibrated model

250 years. The GOF statistics of the March sensitivity to Arctic warming show an RMSE correlation of 0.0037 and a correlation coefficient of 0.99, while the fit against global warming produces a RMSE fit of 0.07. Both statistics suggest the successful performance of our emulator to 2300. We propose the slightly weaker fit to global warming is because this relationship carries the uncertainties from all three steps of our emulator, while the relationship to Arctic warming only carries the uncertainties from one step.
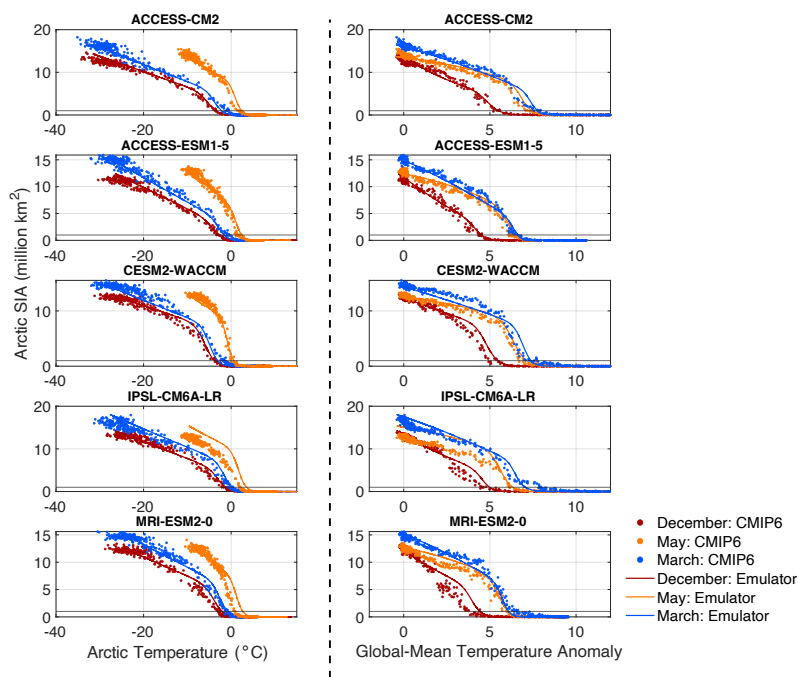
Figure 6. Comparison of the winter sea ice response to Arctic and global warming trends in 'out of sample' extended runs between our emulator and CMIP6 data. The left column shows the SIA response to Arctic warming in extended projections between 1850 and 2300, while the right panel shows the SIA response to global warming in extended projections over the same period. Each row represents one of the five CMIP6 models analysed for each warming trend. Solid lines represent our emulation of the CMIP6 response while scatter points represent the CMIP6 model response. We only show three months here for clarity.

255   Our results suggest that our calibration to 2100 is sufficient to project the non-linearity of winter sea ice loss, however, the
       majority of models analysed indicate that rapid March ice loss occurs after 2100. We attribute this ability of our emulator
       to project the rapid March ice loss, despite it occurring outside the calibration range of our data, to the combination of the
       sigmoidal nature of our SIA parameterisation (Eq. 3b), which inherently assumes the rate of ice loss will increase once the
       threshold temperature controlled by 'b' is reached, and the temperature weighting scheme (Eq. 3a). Although March generally

260   does not warm enough to cause an increase in the rate of ice loss before 2100, the early winter and melt season months
       (November, December and May), show an increase in the sensitivity before 2100. While the specific temperature 'threshold'
       at which the sensitivity increases at varies between the months and models, it is our calibration of the sensitivity in the early
       winter and melt season months that informs ice loss after 2100.

       The Arctic temperature at which rapid ice loss occurs is relatively similar in November and December, whereas the threshold

265   temperature in May is much warmer (Supplementary fig. S7). We attribute this to the different paces in growth and melt of
       Arctic sea ice, discussed in Sect. 2.5.1, suggesting the temperature threshold at which the ice pack detaches from land, causing
       rapid ice loss, will be cooler in the growth season than in the melt season (Ritschel, 2024). Our temperature weighting scheme
       presented in Sect. 2.5.1, (Eq. 3a), parameterises this difference which subsequently updates the threshold temperature of rapid
       ice loss. Without the weighting scheme, the sigmoidal nature of our parameterisation would cause the SIA to decline at the

270   same temperature in each month, at the value set by the sensitivity parameter 'b' (Supplementary fig. S7a). By calibrating to
       the rapid ice loss in the early growth (November and December) and melt season (May) months that exhibit rapid ice loss
       before 2100, our calibration scheme understands the different temperature required to melt and grow ice in both seasons and
       generates a single value for the weight and sensitivity parameters (w and b) to capture the seasonal cycle in each model. Our
       SIA parameterisation then assumes that w and b will have the same effect on the months that don't exhibit rapid ice loss before

275   2100 as the months that do over the calibrated period.

3.2   Reproducing the Observed Sensitivity

       Here we assess whether the constraints we apply to our emulator are sufficient to capture the observed sensitivity of sea ice loss
       to global warming. To do so, we compare our emulator to the 'plausible' range defined by the SIMIP Community (2020), which
       accounts for both the structural and internal variability, by taking two standard deviations of the multi-model CMIP6 ensemble

280   as the uncertainty range around the observed sensitivity of sea ice loss between 1979 and 2014. We take the sensitivity as the
       regression coefficient between the global temperature and SIA projections over the period 1979-2014 (fig. 7). Although our
       emulator generates projections in all months, we focus on the September sensitivity as CMIP6 models tend to underestimate
       the summer sensitivity while reproducing the winter trends relatively well.

       When we constrain our emulator to address both the 'hot model' problem and the Arctic Amplification bias in our emulator, we

285   project a sensitivity than matches the 'plausible' range relatively well in most months. In September, our emulator projects that
       a median of -4.06 million km^2 of sea ice is lost per degree of warming between 1979 and 2014, aligning with the 'plausible'
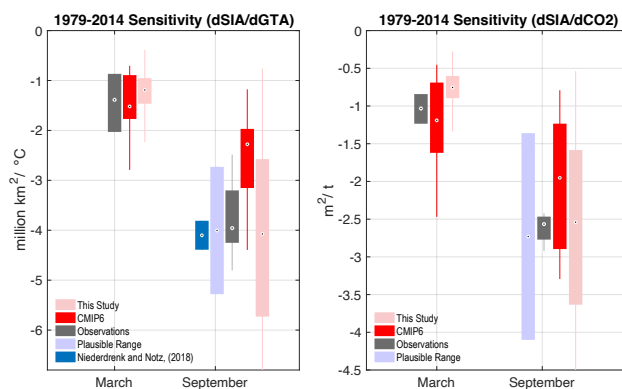
Figure 7. Comparison of the SIA sensitivity to global warming and CO_2 emissions in March and September between our emulator, CMIP6 models and observations. For each month, dark red boxplots denote the sensitivity in CMIP6 models, dark grey boxplots denote the sensitivity from observations, light blue boxes represent the 'plausible' range from observations, light pink boxplots show the sensitivity generated from our observationally constrained emulator, dark blue boxes represent the sensitivity from Niederdrenk and Notz, (2018). All boxplots extend from the lower to upper quartile values over the interquartile range, with a point at the median. Whiskers show the full range of values, excluding outliers.

September sensitivity of -3.95 million km²/°C relatively well. Similarly, when assessing how well our projections aligns with the 'plausible' amount of sea ice loss per metric ton of emitted CO_2, we find our observationally constrained emulator projects a sensitivity of $-2.5\text{m} \pm 0.95\text{m}^2/\text{t}$, which falls within the 'plausible' estimate of $-2.73 \pm 1.37\text{m}^2/\text{t}$. While our interquartile range against global warming is slightly larger than the 'plausible', this is expected due to the probabilistic nature of our emulator and the influence of model uncertainty from CMIP6 multi-model calibration.

3.3 Application: What is the Temperature and Remaining Carbon Budget Necessary to Prevent Arctic Sea Ice Loss Crossing Critical Thresholds?

Through the previous sections we have evidenced that our emulator can reproduce observed sensitivity trends, while also successfully extending projections to 2300. This allows us to apply our emulator to answer key questions in the sea ice discourse. We separate our analysis into two regimes; a linear and non-linear regime. The linear decline of sea ice with cumulative CO_2 emissions in July through to December, which we define as the linear regime, provides the basis for the calculation of a finite remaining carbon budget, alongside and assessment of our current progress towards IPCC warming targets. In a second step, we analyse the non-linear ice loss exhibited in extended projections between January and June, which we define as the non-linear regime, to pinpoint the temperature and CO_2 emission threshold at which winter sea ice detaches from land (Supplementary

fig. S13). While previous studies have assessed the global mean temperature threshold at which rapid winter ice loss occurs, to the best of our knowledge this is the first study to pinpoint the CO_2 emission at which this occurs, over a much wider ensemble range than previously possible.

3.4 Linear Regime
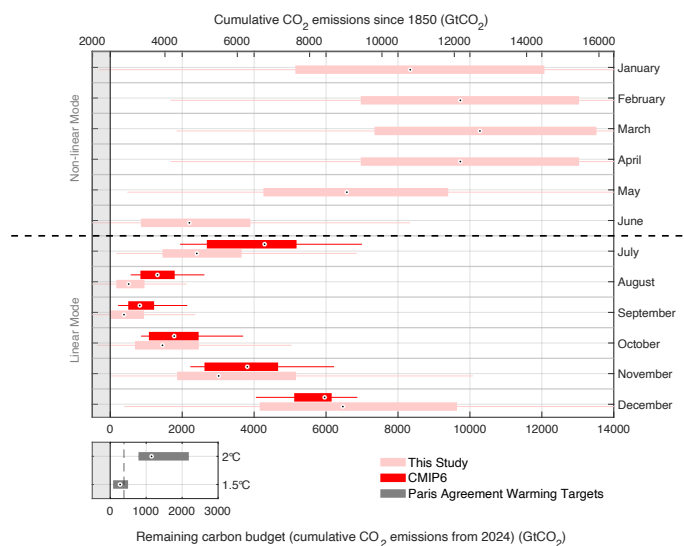
Figure 8. The carbon budget to prevent a seasonally ice-free Arctic Ocean in the linear mode months (July-December) and the carbon budget to prevent rapid ice loss occurring in the non-linear mode months (January-June). Light pink boxplots represent the remaining carbon budgets from 2024, calculated from our emulator. Red boxplots show the remaining carbon budget calculted from the CMIP6 models used in this study. Grey boxplots in the bottom panel compare our results with the remaining carbon budget to prevent Paris Agreement warming targets. The dashed line in the bottom panel compares our emulator's budget for a 50% chance of preventing ice-free conditions in September with the remaining carbon budget to prevent a 1.5°C warming target. Finally, grey vertical shading represents carbon emissions that would exceed the budget to prevent an ice-free ocean or to prevent non-linear ice loss in the winter months. Boxplots represent the interquartile range of the data with the median shown through the black and white dot.

305   When translating the constrained sensitivity from our emulator into the remaining carbon budget, we estimate that there is a 50% chance Arctic September sea ice will be lost for an additional 380 Gt of CO_2 emissions from 2024 (fig. 8) (IQR: -14GtCO$_2$ and 940 GtCO$_2$). Our estimate is smaller than CMIP6 projections, which suggest a median of 821GtCO$_2$ (IQR: 500GtCO$_2$ and 1220GtCO$_2$) will cause a seasonally ice-free Arctic Ocean. If we assume the average current emission trends of 38Gt of CO_2

per year will continue into the future (Lamboll et al., 2023), our updated limit of $380\,\mathrm{GtCO_2}$ will be reached within the next

310   decade.
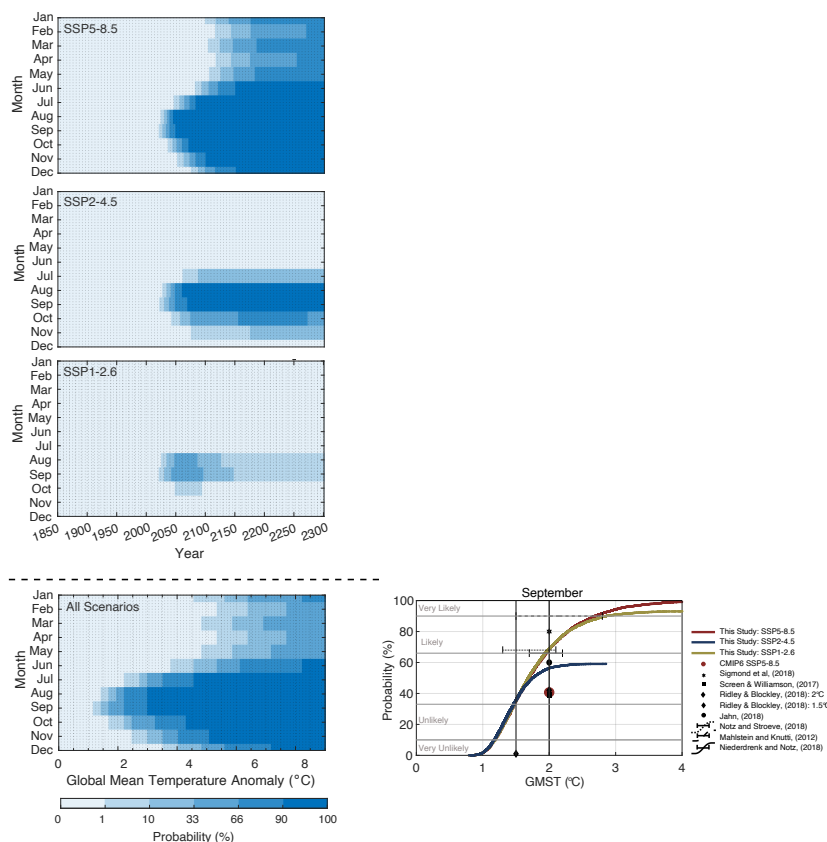
Figure 9. The probability of ice-free conditions in each month, year and global mean temperature by 2300 generated from our observationally constrained emulator. The probability in each year under SSP5-8.5, SSP2-4.5 and SSP1-2.6 are given in the upper three panels. The probability as a function of global temperature is shown in the bottom panel, and is calculated from the likelihood of ice-free conditions at each global temperature under all three scenarios combined. Darker blue patches represent increasingly ice-free conditions, while whiter patches indicate years and temperatures where a high percentage of emulator ensemble members project high ice cover above 1 million square kilometers. The right panel represents the cumulative probability of the global mean temperature at which the SIA falls below 1 million $\mathrm{km^2}$ for the first time in our observationally constrained emulator. Red, yellow and blue represent SSP5-8.5, SSP2-4.5 and SSP1-2.6 respectively. Errorbars and scattered shapes represent probability ranges from other studies.

Our analysis indicates that, at the lower bound, we have surpassed the remaining carbon budget by 14Gt of CO_2, implying that sufficient carbon has already been emitted to cause a seasonally ice-free Arctic Ocean. However, observational data suggests this is an overestimate as the Arctic Ocean has not yet exhibited seasonally ice-free conditions. We attribute the overestimate to the broader range of our emulator's 2024 SIA projections compared to the more constrained observed values. Although

315   our emulator considers the full range of observed data, its range is larger than the observed as the 2024 SIA shows very little variation across the available observational datasets. This variance likely arises because our model is calibrated to the 1850–2100 period over the CMIP6 multi-model range, rather than specifically to the year 2024. Calculating the remaining carbon budget using the same sensitivity and the lower bound of our projected 2024 SIA will produce a smaller budget than the same sensitivity applied to a larger 2024 observed SIA value. This could explain why the lower limit of our emulator range

320   overestimates the carbon budget although the sensitivities align. If we had calibrated our emulator to match the observed SIA in September 2023 (3.8 million km^2), our sensitivity range would suggest a remaining $235GtCO_2$ - $1737GtCO_2$ could be emitted before ice-free conditions occur.

Assessing our carbon budgets against IPCC warming targets reveals that the median remaining carbon budget to prevent an ice-free Arctic Ocean in September is larger than the budget for limiting global warming to 1.5°C (275 $GtCO_2$), yet smaller

325   than the budget limiting warming to 2°C (1150 $GtCO_2$) (fig. 9) (Friedlingstein et al., 2023; Lamboll et al., 2023). Under a high and medium emission scenario (SSP5-8.5 and SSP2-4.5), our emulator projects SIA will *likely* (IPCC likelihood scale defined in the Supplementary material, Sect. S2.2) become ice-free at 1.9°C, whereas only 38% of ensembles project an ice-free Arctic Ocean in September at 1.5°C. Interestingly, the probability of an ice-free ocean under a low emission scenario (SSP1-2.6) significantly increases when constraining the sensitivity. Although the probability does not become *likely* by the

330   IPCC definition of 66%, the probability peaks at 59% in 2068 before declining as SIA recovers (fig. 9).

3.5   Non-linear Regime

Our emulator suggests that March sea ice declines slowly with CO_2 initially, at a rate of -0.75m^2/t (IQR: -0.6 to -0.91m^2/t) per emitted ton of CO_2 up to a threshold emission of approximately $10,000GtCO_2$ from 2024 (IQR: $7156GtCO_2$ to $13,596$ $GtCO_2$), after which the sensitivity increases to a rate of -2.2m^2/t (IQR: -1.75 to -2.93m^2/t) (fig. 8). The emission threshold

335   we identify corresponds to a median global mean temperature of 5.42°C (IQR: 4.349°C – 6.62°C) (fig. 9). Once the emission/ temperature threshold is exceeded, the Arctic ice pack will detach from land year-round, increasing the sensitivity at which sea ice is lost to cumulative carbon emissions. After this threshold has been reached the Arctic Ocean opens up rapidly.

While SIA tends to decline with CO_2 emissions at the same rate across all scenarios, rapid ice loss only occurs under the high-emission scenario (SSP5-8.5), while the emission reductions in other scenarios prevent the majority of ensembles reaching the

340   thresholds we identify.

4 Discussion

In this study, we present an Arctic sea ice emulator that efficiently generates long-term probabilistic projections of sea ice that capture current trends and the latest physical understanding of the sea ice system from CMIP6 models. We have demonstrated how our emulator uses a comparatively simple set of parameterisations to empirically capture the key features of SIA loss with global warming, compared to the complexity, detailed physics and computational costs of CMIP6 models. Building on this foundation, we show that applying constraints to address the 'hot model' problem and underestimation of Arctic Amplification in CMIP6 models, enables our emulator to generate SIA projections that reproduce the 'plausible' (observationally derived) sensitivity well. We highlight that our observational constraint on Arctic Amplification is key to aligning our emulator's sensitivity with observations, as the sensitivity generated from projections forced by the MAGICC temperature and the CMIP6 calibrated Arctic Amplification do not align with observational data. This suggests that the degree of Arctic amplification in climate models may be key to understanding the future of Arctic sea ice.

Our constrained emulator reduces the remaining carbon budget to prevent a seasonally ice-free Arctic Ocean from CMIP6 estimates by 441GtCO$_2$ from 2024 at its median. This suggests that limiting global warming to 1.5°C (275 GtCO$_2$) is sufficient to prevent a seasonally ice-free Arctic Ocean, whereas 2°C (1150 GtCO$_2$) proves insufficient. These findings indicate greater emission reductions may be required than current policy solutions suggest. While earlier studies have constrained the timing of an ice-free ocean, most recalibrate the modelled Arctic sea ice output, linearly extrapolate observations to ice-free conditions, or select climate models based on their ability to reproduce the observed rate of sea ice loss (Winton, 2011; Niederdrenk and Notz, 2018; Wang et al., 2021; Sigmond et al., 2018; Kim et al., 2023; Jahn et al., 2024; Poltronieri et al., 2022). These methods conclude that ice-free conditions in September are *likely* at 1.8°C with a range between 1.3°C and 2.9°C of global warming (9). Our results agree well with these approaches projecting a *likely* ocean at 1.89°C.

Another crucial insight has been the ability of our emulator to capture the rapid loss of winter sea ice to warming outside of the calibration period, from a more extensive ensemble than CMIP6 models are currently able to achieve. We find there is a 50% chance of sea ice detaching from land in March for the emission of a remaining 10,000GtCO$_2$ from 2024, corresponding to a global mean temperature of 5.42°C (IQR: 3.9°C - 6.3°C). When comparing to previous findings, our emulator identifies a threshold that is slightly higher than found by Meccia et al. (2020), who use computationally efficient stochastic physics schemes to project rapid winter sea ice loss will occur at 4 $\pm$ 0.35°C of global warming. Whereas our threshold falls within the lower range from Drijfhout et al. (2015), who use five CMIP5 model simulations (due to the lack of extended runs past 2100) to suggest the threshold occurs at a global mean temperature ranging between 4.5°C and 8.2°C. Our results add to this body of work by providing a more thorough assessment of winter ice loss backed by a wider range of CMIP6 models and observations, which potentially accounts for the slightly different threshold global temperature from our emulator, than the two studies discussed here.

While our constraint on Arctic Amplification assumes the ratio will remain constant through the simulation period, some CMIP6 models suggest that the Arctic Amplification will decline as sea ice retreats (Dai et al., 2019; Holland and Landrum, 2021). As the amount of remaining sea ice is usually low or ice-free before it impacts the Arctic Amplification in summer,

375   the feedback mechanism would have minimal influence on our model's projections during this season. Whereas in winter, the rate of sea ice loss after the ice pack detaches from land is so high that changes to the Arctic Amplification past this time have little impact on our SIA projections. While we have shown our constrained Arctic Amplification trend increases the likelihood of an ice-free ocean at lower emission levels compared to CMIP6 estimates, its future is uncertain. It is possible our emulator projects a conservative estimate of future Arctic Amplification if current trends continue to persist. If so, the Arctic Ocean could

380   become ice-free earlier than our current projections suggest. In addition, recent studies suggest a non-negligable portion of sea ice loss is a result of internal tropical-polar teleconnections, that CMIP6 models and therefore our emulator don't currently capture (Baxter and Ding, 2022; Topál and Ding, 2023). It would be interesting for further work to investigate the contribution of polar-tropical teleconnections to sea ice variability in long-term projections, to determine if this could increase the remaining carbon budget we project will prevent ice-free conditions.

385   ## 5 Conclusions

This study has presented a novel method of probabilistic sea ice projection through the development and application of an Arctic sea ice emulator. Our emulator's ability to efficiently extend future seasonal SIA based on the present sensitivity to global temperatures while also considering the range of knowledge within CMIP6 models, proves its use as a tool to answer prominent questions regarding the future of Arctic sea ice. This method fills the gap in the literature between complex CMIP6

390   projections, recalibration of model output, and the simple linear extrapolation of sea ice area with anthropogenic forcing. The results from the application of our emulator bring into question whether mitigation efforts are stringent enough to prevent critical ice loss, while also providing useful information regarding regime changes in sea ice loss that could cause ice-free conditions to occur rapidly year-round.

Code availability. https://doi.org/10.5281/zenodo.14020702

395   *Data availability.* The observational Arctic Amplification evolution is analysed through three datasets. NASA's Goddard Institute for Space Studies Surface Temperature version 4 (GISTEMP) with a 1200km smoothing radius (Lenssen et al. (2019)), the Berkeley Earth temperature dataset (BEST) (Rohde and Hausfather (2020)) and the Met Office Hadley Centre/Climatic Research Unit version 5.0.1.0 (HadCRUT5) dataset (Morice et al. (2021)). The HADCRUT temperature range was obtained from the 200 member ensemble. In these datasets, near-surface air temperature is based on a combination of 2m temperature observations over land and sea surface temperature (SST) observations

400   over the ocean. The global mean temperature anomaly is defined as the average temperature across the gridded dataset while the Arctic

temperature anomaly counterpart is defined as the average of the area poleward of 65°N. Arctic absolute seasonal temperature observations are downloaded as a time series from the Berkeley product. Observational Northern hemispheric SIA datasets are those from the University of Hamburg (UHH) Sea Ice Area Product (Doerr et al. (2021)). The six products used include: the HadISST NSIDC monthly sea-ice area; HadISST original monthly sea-ice area; Comiso-Bootstrap monthly sea-ice area; NASA-Team monthly sea-ice area; OSI-SAF monthly sea-

405 ice area and the Walsh monthly sea-ice area. Cumulative CO_2 emission projections are taken from the historical fossil fuel and industrial datasets that were used for harmonising IPCC emissions scenarios (IPCC (2022), AR6 WG3; Nicholls et al. (2020), RCMIP datasetes). As the cumulative CO_2 emission projections begin in 1750, to analyse the remaining carbon budget from 2023 we simply subtract the cumulative CO_2 emission in 2023 from the total carbon budget in each ensemble.

Author contributions. SC and MM conceptualised the study. SC conducted data collection, analysis, and validation and served as the primary

410 developer of the emulator parameterisations, with co-development and supervision from MM. SC also performed the model application analyses and prepared the initial manuscript draft, while MM contributed to manuscript review and editing.

Competing interests. The contact author has declared that none of the authors has any competing interests.

Acknowledgements. This work would not have been possible without the expertise, dedication, and guidance of Dirk Notz, PhD supervisor to SC. We are also deeply grateful to Peter Rayner for his invaluable support and advice throughout this project. SC's work was funded by the

415 Melbourne Research Scholarship and the Dr. Albert Shimmins Fund. Finally, we extend our thanks to the many individuals whose dedication made the datasets used in this study possible.

References

Armour, K. C., Eisenman, I., Blanchard-Wrigglesworth, E., McCusker, K. E., and Bitz, C. M.: The reversibility of sea ice loss in a state-of-the-art climate model, Geophysical Research Letters, 38, https://doi.org/10.1029/2011GL048739, 2011.

420 Balaji, V., Maisonnave, E., Zadeh, N., Lawrence, B. N., Biercamp, J., Fladrich, U., Aloisio, G., Benson, R., Caubel, A., Durachta, J., et al.: CPMIP: measurements of real computational performance of Earth system models in CMIP6, Geoscientific Model Development, 10, 19–34, 2017.

Bathiany, S., Notz, D., Mauritsen, T., Raedel, G., and Brovkin, V.: On the Potential for Abrupt Arctic Winter Sea Ice Loss, Journal of Climate, https://doi.org/10.1175/JCLI-D-15, 2016.

425 Baxter, I. and Ding, Q.: An optimal atmospheric circulation mode in the Arctic favoring strong Summertime Sea ice melting and ice–albedo feedback, Journal of Climate, 35, 6627–6645, 2022.

Bonan, D. B., Lehner, F., and Holland, M. M.: Partitioning uncertainty in projections of Arctic sea ice, Environmental Research Letters, 16, https://doi.org/10.1088/1748-9326/abe0ec, 2021.

Chylek, P., Folland, C., Klett, J. D., Wang, M., Hengartner, N., Lesins, G., and Dubey, M. K.: Annual Mean Arctic Amplification 1970–2020:
430 Observed and Simulated by CMIP6 Climate Models, Geophysical Research Letters, 49, https://doi.org/10.1029/2022GL099371, 2022.

Chylek, P., Folland, C. K., Klett, J. D., Wang, M., Lesins, G., and Dubey, M. K.: High Values of the Arctic Amplification in the Early Decades of the 21st Century: Causes of Discrepancy by CMIP6 Models Between Observation and Simulation, Journal of Geophysical Research: Atmospheres, 128, https://doi.org/10.1029/2023JD039269, 2023.

Dai, A., Luo, D., Song, M., and Liu, J.: Arctic amplification is caused by sea-ice loss under increasing CO2, Nature Communications, 10,
435 https://doi.org/10.1038/s41467-018-07954-9, 2019.

DeRepentigny, P., Jahn, A., Holland, M. M., and Smith, A.: Arctic sea ice in two configurations of the CESM2 during the 20th and 21st centuries, Journal of Geophysical Research: Oceans, 125, e2020JC016 133, 2020.

Doerr, J., Notz, D., and Kern, S.: UHH Sea Ice Area Product, 2021.

Douville: Robust and perfectible constraints on human-induced Arctic amplification, Communications Earth and Environment, 4,
440 https://doi.org/10.1038/s43247-023-00949-5, 2023.

Drijfhout, S., Bathiany, S., Beaulieu, C., Brovkin, V., Claussen, M., Huntingford, C., Scheffer, M., Sgubin, G., and Swingedouw, D.: Catalogue of abrupt shifts in Intergovernmental Panel on Climate Change climate models, Proceedings of the National Academy of Sciences of the United States of America, 112, E5777–E5786, https://doi.org/10.1073/pnas.1511451112, 2015.

Eisenman: Geographic muting of changes in the Arctic sea ice cover, Geophysical Research Letters, 37,
445 https://doi.org/10.1029/2010GL043741, 2010.

Friedlingstein, P., O'Sullivan, M., Jones, M. W., Andrew, R. M., Bakker, D. C., Hauck, J., Landschützer, P., Quéré, C. L., Luijkx, I. T., Peters, G. P., Peters, W., Pongratz, J., Schwingshackl, C., Sitch, S., Canadell, J. G., Ciais, P., Jackson, R. B., Alin, S. R., Anthoni, P., Barbero, L., Bates, N. R., Becker, M., Bellouin, N., Decharme, B., Bopp, L., Brasika, I. B. M., Cadule, P., Chamberlain, M. A., Chandra, N., Chau, T. T. T., Chevallier, F., Chini, L. P., Cronin, M., Dou, X., Enyo, K., Evans, W., Falk, S., Feely, R. A., Feng, L., Ford, D. J., Gasser, T., Ghattas,
450 J., Gkritzalis, T., Grassi, G., Gregor, L., Gruber, N., Özgür Gürses, Harris, I., Hefner, M., Heinke, J., Houghton, R. A., Hurtt, G. C., Iida, Y., Ilyina, T., Jacobson, A. R., Jain, A., Jarníková, T., Jersild, A., Jiang, F., Jin, Z., Joos, F., Kato, E., Keeling, R. F., Kennedy, D., Goldewijk, K. K., Knauer, J., Korsbakken, J. I., Körtzinger, A., Lan, X., Lefèvre, N., Li, H., Liu, J., Liu, Z., Ma, L., Marland, G., Mayot, N., McGuire, P. C., McKinley, G. A., Meyer, G., Morgan, E. J., Munro, D. R., Nakaoka, S. I., Niwa, Y., O'Brien, K. M., Olsen, A., Omar,

A. M., Ono, T., Paulsen, M., Pierrot, D., Pocock, K., Poulter, B., Powis, C. M., Rehder, G., Resplandy, L., Robertson, E., Rödenbeck,

455   C., Rosan, T. M., Schwinger, J., Séférian, R., Smallman, T. L., Smith, S. M., Sospedra-Alfonso, R., Sun, Q., Sutton, A. J., Sweeney, C.,
Takao, S., Tans, P. P., Tian, H., Tilbrook, B., Tsujino, H., Tubiello, F., van der Werf, G. R., van Ooijen, E., Wanninkhof, R., Watanabe,
M., Wimart-Rousseau, C., Yang, D., Yang, X., Yuan, W., Yue, X., Zaehle, S., Zeng, J., and Zheng, B.: Global Carbon Budget 2023, Earth
System Science Data, 15, 5301–5369, https://doi.org/10.5194/essd-15-5301-2023, 2023.

Hankel, C. and Tziperman, E.: The Role of Atmospheric Feedbacks in Abrupt Winter Arctic Sea Ice Loss in Future Warming Scenarios,

460   Journal of Climate, https://doi.org/10.1175/JCLI-D-20, 2021.

Hankel, C. and Tziperman, E.: An approach for projecting the timing of abrupt winter Arctic sea ice loss, Nonlinear Processes in Geophysics,
30, 299–309, https://doi.org/10.5194/npg-30-299-2023, 2023.

Hausfather, Marvel, Schmidt, Nielsen-Gammon, and Zelinka: Climate simulations: recognize the 'hot model' problem Setting the agenda in
research, Nature, 26, 2022.

465   Hay, S., Screen, J., and Catto, J. L.: Steady but model dependent Arctic amplification of the forced temperature response in 21st century
CMIP6 projections, Environmental Research: Climate, https://doi.org/10.1088/2752-5295/ad4201, 2024.

Hezel, P. J., Fichefet, T., and Massonnet, F.: Modeled Arctic sea ice evolution through 2300 in CMIP5 extended RCPs, Cryosphere, 8,
1195–1204, https://doi.org/10.5194/tc-8-1195-2014, 2014.

Holland, M. M. and Landrum, L.: The Emergence and Transient Nature of Arctic Amplification in Coupled Climate Models, Frontiers in

470   Earth Science, 9, https://doi.org/10.3389/feart.2021.719024, 2021.

IPCC: Climate Change 2021: The Physical Science Basis. Contribution of Working Group I to the Sixth Assessment Report of the Intergov-
ernmental Panel on Climate Change, vol. In Press, Cambridge University Press, Cambridge, United Kingdom and New York, NY, USA,
https://doi.org/10.1017/9781009157896, 2021.

IPCC: Climate Change 2022: Mitigation of Climate Change. Contribution of Working Group III to the Sixth Assessment Report

475   of the Intergovernmental Panel on Climate Change, Cambridge University Press, Cambridge, UK and New York, NY, USA,
https://doi.org/10.1017/9781009157926, 2022.

Jahn, A., Holland, M. M., and Kay, J. E.: Projections of an ice-free Arctic Ocean, Nature Reviews Earth and Environment, 5, 164–176,
https://doi.org/10.1038/s43017-023-00515-9, 2024.

Kim, Y. H., Min, S. K., Gillett, N. P., Notz, D., and Malinina, E.: Observationally-constrained projections of an ice-free Arctic even under a

480   low emission scenario, Nature Communications, 14, https://doi.org/10.1038/s41467-023-38511-8, 2023.

Lagarias, J. C., Reeds, J. A., Wright, M. H., Wright, P. E., and Optim, S. J.: Convergence Properties of the Nelder-Mean Simplex Method in
Low Dimensions, Society for Industrial and Applied Mathematics, 9, 112–147, http://www.siam.org/journals/ojsa.php, 1998.

Lamboll, R. D., Nicholls, Z. R., Smith, C. J., Kikstra, J. S., Byers, E., and Rogelj, J.: Assessing the size and uncertainty of remaining carbon
budgets, Nature Climate Change, 13, 1360–1367, https://doi.org/10.1038/s41558-023-01848-5, 2023.

485   Lenssen, N. J., Schmidt, G. A., Hansen, J. E., Menne, M. J., Persin, A., Ruedy, R., and Zyss, D.: Improvements in the GISTEMP uncertainty
model, Journal of Geophysical Research: Atmospheres, 124, 6307–6326, 2019.

Mahlstein, I. and Knutti, R.: September Arctic sea ice predicted to disappear near 2°C global warming above present, Journal of Geophysical
Research Atmospheres, 117, https://doi.org/10.1029/2011JD016709, 2012.

Meccia, V. L., Fabiano, F., Davini, P., and Corti, S.: Stochastic Parameterizations and the Climate Response to External Forcing: An Experi-

490   ment With EC-Earth, Geophysical Research Letters, 47, https://doi.org/10.1029/2019GL085951, 2020.

Morice, C. P., Kennedy, J. J., Rayner, N. A., Winn, J., Hogan, E., Killick, R., Dunn, R., Osborn, T., Jones, P., and Simpson, I.: An updated assessment of near-surface temperature change from 1850: The HadCRUT5 data set, Journal of Geophysical Research: Atmospheres, 126, e2019JD032 361, 2021.

Nelder, J. A. and Meadf, R.: A simplex method for function minimization, The Computer Journal, 7, 308–313, http://comjnl.oxfordjournals.
495   org/, 1965.

Nicholls, Z., Meinshausen, M., Lewis, J., Gieseke, R., Dommenget, D., Dorheim, K., Fan, C.-S., Fuglestvedt, J., Gasser, T., and Golüke, U.: Reduced Complexity Model Intercomparison Project Phase 1: introduction and evaluation of global-mean temperature response, Geoscientific Model Development, https://doi.org/10.5194/gmd, 2020.

Nicholls, Z., Meinshausen, M., Lewis, J., Corradi, M. R., Dorheim, K., Gasser, T., Gieseke, R., Hope, A. P., Leach, N. J., McBride, L. A.,
500   Quilcaille, Y., Rogelj, J., Salawitch, R. J., Samset, B. H., Sandstad, M., Shiklomanov, A., Skeie, R. B., Smith, C. J., Smith, S. J., Su, X., Tsutsui, J., Vega-Westhoff, B., and Woodard, D. L.: Reduced Complexity Model Intercomparison Project Phase 2: Synthesizing Earth System Knowledge for Probabilistic Climate Projections, Earth's Future, 9, https://doi.org/10.1029/2020EF001900, 2021.

Niederdrenk and Notz: Arctic Sea Ice in a 1.5°C Warmer World, Geophysical Research Letters, 45, 1963–1971, https://doi.org/10.1002/2017GL076159, 2018.

505   Poltronieri, A., Bochow, N., Aksamit, N. O., Boers, N., Jakobsen, P., and Rypdal, M.: Arctic summer sea ice loss will accelerate in coming decades, Environmental Research Letters, 2022.

Rantanen, Karpechko, Lipponen, Nordling, Hyvärinen, Ruosteenoja, Vihma, and Laaksonen: The Arctic has warmed nearly four times faster than the globe since 1979, Communications Earth and Environment, 3, https://doi.org/10.1038/s43247-022-00498-3, 2022.

Ritschel: A transforming Arctic: Unraveling Climate Change Impacts on Sea Ice Dynamics and Oceanic pCO2, https://orcid.org/
510   0000-0001-7464-7075, 2024.

Rohde, R. A. and Hausfather, Z.: The Berkeley Earth land/ocean temperature record, Earth System Science Data, 12, 3469–3479, 2020.

Rosenblum and Eisenman: Sea Ice Trends in Climate Models Only Accurate in Runs with Biased Global Warming, Journal of Climate, https://doi.org/10.1175/JCLI-D-16-0455.s1, 2017.

Serreze and Barry: Processes and impacts of Arctic amplification: A research synthesis, Global and Planetary Change, 77, 85–96,
515   https://doi.org/10.1016/j.gloplacha.2011.03.004, 2011.

Serreze and Stroeve: Arctic sea ice trends, variability and implications for seasonal ice forecasting, Philosophical Transactions of the Royal Society A: Mathematical, Physical and Engineering Sciences, 373, https://doi.org/10.1098/rsta.2014.0159, 2015.

Sigmond, M., Fyfe, J. C., and Swart, N. C.: Ice-free Arctic projections under the Paris Agreement, Nature Climate Change, 8, 404–408, https://doi.org/10.1038/s41558-018-0124-y, 2018.

520   SIMIP Community: Arctic Sea Ice in CMIP6, Geophysical Research Letters, 47, https://doi.org/10.1029/2019GL086749, 2020.

Topál, D. and Ding, Q.: Atmospheric circulation-constrained model sensitivity recalibrates Arctic climate projections, Nature Climate Change, 13, 710–718, 2023.

Wang, B., Zhou, X., Ding, Q., and Liu, J.: Increasing confidence in projecting the Arctic ice-free year with emergent constraints, Environmental Research Letters, 16, https://doi.org/10.1088/1748-9326/ac0b17, 2021.

525   Winton, M.: Do climate models underestimate the sensitivity of Northern Hemisphere sea ice cover?, Journal of Climate, 24, 3924–3934, https://doi.org/10.1175/2011JCLI4146.1, 2011.